Decadal Changes in Meridional Overturning Circulation in the East Sea (Sea of Japan)

MYEONGHEE HAN AND YANG-KI CHO

School of Earth and Environmental Sciences, and Research Institute of Oceanography, Seoul National University, Seoul, South Korea

HYOUN-WOO KANG

Ocean Circulation and Climate Research Center, Korea Institute of Ocean Science and Technology, Busan, South Korea

SUNGHYUN NAM

School of Earth and Environmental Sciences, and Research Institute of Oceanography, Seoul National University, Seoul, South Korea

(Manuscript received 15 October 2019, in final form 27 March 2020)

ABSTRACT

Meridional overturning circulation (MOC) is vital to distributing heat, freshwater, and dissolved matter in semienclosed deep marginal seas such as the East Sea (ES) (Sea of Japan). As our understanding of the ES MOC remains incomplete, we attempted to fill this research gap. We analyzed the ES MOC and its decadal change (1993–2012), employing Hybrid Coordinate Ocean Model (HYCOM) global reanalysis. We found that the ES MOC, consisting of two counterrotating overturning cells in the late 1990s, changed into a single full-depth cell in the 2000s and reverted to two cells in the 2010s. The decadal change relates to weakening of the southward western boundary current at the intermediate layer and northward eastern boundary currents at the deep abyssal layer. We propose that surface warming and salinification favored reduced intermediate water formation and enhanced bottom water formation in the northwestern ES in the 2000s and were, therefore, key to the decadal change. Conditions unfavorable to intermediate water formation and favorable to bottom water formation in the winters of the 2000s, compared with the late 1990s, enhanced northward (westward) Ekman transport in the southern (northeastern) ES, successive advection of surface warm, saline water into water formation areas, and air–sea heat and freshwater exchanges linked to the January Arctic Oscillation. Our results indicated that the ES MOC is sensitive to both external atmospheric forcing and internal ES processes, which have implications for significant changes in the response of other marginal seas and global oceans to future climate variability.

1. Introduction

Global meridional overturning circulation (MOC), often based on zonally and vertically integrated meridional flows in the ocean, carries an extremely large amount of heat from low- to high-latitude regions, contributing to the overall climate of Earth (Wunsch 2002; Stouffer et al. 2006). In contrast to the increased interest in the Atlantic MOC, the Pacific MOC has not attracted significant attention, as it features from near-unventilated surface waters to a deep and abyssal layer, e.g., low dissolved oxygen at 1000 m (Talley et al. 2006). However, there is an exception in one of the marginal seas in the North Pacific, namely, the East Sea (ES) (Sea of Japan). Here, as it is connected to the Pacific via relatively narrow and shallow straits (Fig. 1), diverse processes work to vigorously ventilate the sea. These processes occur in response to changes in the surface atmospheric and oceanic conditions, and intrinsic internal circulation with a rapid overturn time scale (<100 years), which yield the highest levels of deep dissolved oxygen in the Pacific, including the South Pacific (e.g., Kim et al. 2004; Talley et al. 2006; Yoon et al. 2018).

The ES is a small, semienclosed deep basin (>3000 m) consisting of three basins, namely, the Japan Basin (JB),

Denotes content that is immediately available upon publication as open access.

Corresponding author: SungHyun Nam, namsh@snu.ac.kr

DOI: 10.1175/JPO-D-19-0248.1

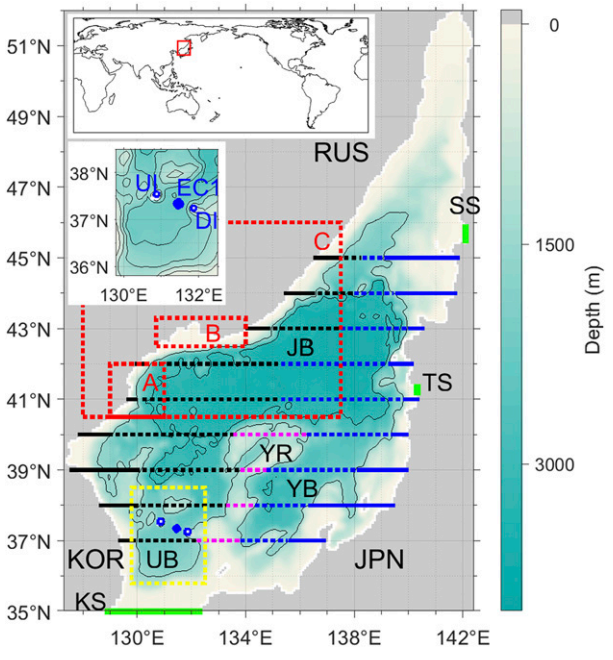

FIG. 1. Bathymetry of the East Sea (ES) (Sea of Japan) with color scale on right (contour interval: 1500 m). KOR, JPN, and RUS denote South Korea, Japan, and Russia, respectively, and UB, YB, YR, and JB indicate the Ulleung Basin, Yamato Basin, Yamato Ridge, and Japan Basin, respectively. KS, TS, and SS indicated by green lines represent the Korea–Tsushima Strait, Tsugaru Strait, and Soya Straits, respectively. Three selected areas, area A (129.0°–131.0°E and 40.5°–42.0°N), area B (130.7°–134.0°E and 42.5°–43.3°N), and area C (128.0°–137.5°E and 40.5°–46.0°N) are marked with red dashed boxes. The zonal sections at 37°–45°N are separated into four or five subsections: western boundaries shallower than 1500-m depth (black solid lines), western troughs deeper than 1500 m (black dashed lines), middle ridges shallower than 1500 m (magenta dashed lines), eastern troughs deeper than 1500 m (blue dashed lines), and eastern boundaries shallower than 1500 m (blue solid lines). The red rectangle in the upper map denotes the study area. The UB area marked with a yellow dashed box is zoomed-in in the upper-left corner with bathymetry (contour interval: 500 m), and the names of islands and mooring (UI: Ulleung Island, EC1: mooring, DI: Dok Island).

Ulleung Basin (UB), and Yamato Basin (YB) in the northwest Pacific (Fig. 1). The severe ventilation in this almost isolated deep basin and its temporal changes are correlated with the variability in the intensity and structure of its own MOC (hereafter referred to as the ES MOC). Furthermore, the ES MOC and its variability make critical contributions to the regional climate and ecosystem variability through the distribution of heat, buoyancy, and dissolved matter, and have implications for the global MOC as a "miniature ocean" (Ichiye 1984; Kim et al. 2002; Talley et al. 2003). However, the ES MOC and its variability remain largely unexplored, with only a small number of previous studies having addressed the formation and characteristics of deep water and both intermediate and deep circulations in the ES, and even fewer having investigated the ES MOC.

The overall structures and characteristics of the ES water masses and their changes have been observed and investigated over many decades (e.g., Miyazaki 1953; Moriyasu 1972; Kim and Chung 1984; Kim and Kim 1999; Kim et al. 2004; Talley et al. 2006; Chang et al. 2016; Yoon et al. 2018). The ES has an inlet and outlet system in which the inflow transports warm and saline water, named the Tsushima Warm Water (TWW), into the sea through the Korea–Tsushima Strait (KS). This is generally balanced by outflows through the Tsugaru Strait (TS) and Soya Strait (SS) (Fig. 1). Therefore, upper circulation patterns are generated by this system (Cho et al. 2009). In the western ES, the East Sea Intermediate Water (ESIW) or North Korea Cold Water (NKCW), characterized by a vertical salinity minimum (Kim and Chung 1984; Kim and Kim 1999; Kim et al. 2004; Talley et al. 2006; Chang et al. 2016; Nam et al. 2016), has been found at an intermediate layer, e.g., depth from a couple to a few hundred meters, as confirmed by hydrographic observations. Below the ESIW, three deep-water masses have been identified from hydrographic observations, particularly in the northern JB according to, e.g., Kim et al. (2004). A distinct deep salinity minimum located at approximately 1500 m divides the Central Water (CW) above and the Deep Water (DW) below the layer. The abyssal layer is occupied by the Bottom Water (BW), identified by a vertically homogeneous layer (Kim et al. 2004; Talley et al. 2006; Chang et al. 2016; Yoon et al. 2018).

The properties, formations, volumes, and spatial distributions of these water masses demonstrate strong temporal variability on decadal, interannual, and annual time scales. In detail, 1) the ESIW forms every winter as a mixed layer water, subducted in the northwestern ES (area A in Fig. 1) and transported toward the KS by the southward-flowing North Korea Cold Current (NKCC) (Cho and Kim 1998; Kim and Kim 1999; Yoshikawa et al. 1999; Yun et al. 2004; Kim et al. 2006; Min and Kim 2006; Park and Lim 2017); 2) decadal changes in the dense CW, DW, and BW formations occur via open-ocean convection and deep-slope convection in response to convective mixing, saline water transport, freshwater loss to atmosphere (evaporation minus precipitation), and sea ice formation that yield brine rejection (Noh and Jang 1999; Kang et al. 2003; Talley et al. 2003; Kim et al. 2004; Cui and Senjyu 2010; Yoon et al. 2018); and 3) decadal and interannual variability of the ESIW properties are apparent, associated with the Arctic Oscillation (AO), wintertime air–sea heat exchanges in the northern ES, and circulation in the southwestern ES (Cui and Senjyu 2010; Tanaka 2014;

Nam et al. 2016). However, surprisingly few studies have addressed the ES MOC, and only a seasonal reversal of deep overturning circulation associated with wind-driven Ekman pumping and geothermal effects on 40-yr mean ES MOC were suggested by numerical models (Yoshikawa et al. 1999; Park et al. 2013). Decadal changes in the ES MOC have not been examined, either from observations or by numerical modeling.

In this study, we attempted to address the mean structure and intensity of the ES MOC and its temporal changes, with emphasis on the decadal change, identified from relatively well-validated global reanalysis products in comparison with in situ observations of the ES. The data and methods are described in section 2, and the results and discussion are presented in sections 3 and 4, respectively. The summary and conclusions are given in section 5.

2. Data and methods

a. Data sources

The Hybrid Coordinate Ocean Model (HYCOM) global reanalysis product (GLBb0.08), with Navy Coupled Ocean Data Assimilation (NCODA), has a horizontal resolution of 0.08° and employs a hybrid coordinate in which three vertical coordinates, namely, isobars (pressure), isopycnals (density), and sigma levels (terrain) are used simultaneously. In this study, we analyzed the monthly mean original data on temperature, salinity, density, and horizontal current given by the HYCOM products in the ES (Fig. 1) for the period 1993–2012. To estimate surface fluxes of heat, freshwater, buoyancy, and momentum (Ekman transport), we used the monthly mean data of the surface shortwave and longwave radiations, sensible and latent heat fluxes, evaporation, precipitation, and wind stress from the Modern-Era Retrospective Analysis for Research and Applications, version 2 (MERRA-2).

To validate the HYCOM data, we used three types of in situ observational data collected for the target period 1993–2012, namely, 1) ferry-mounted acoustic Doppler current profiler (ADCP) data collected across the KS between Busan, South Korea, and Fukuoka, Japan; 2) serial hydrographic data collected bimonthly off the east coast of South Korea; and 3) deep current-meter data collected by the EC1 mooring located at 131.5°E and 37.3°N between Ulleung Island (UI) and Dok Island (DI), as well as by other moorings. All EC1 mooring data are available to the general public, as well as the science community (Noh and Nam 2018). The volume transport across the KS (V_{obs}) was estimated from the ferry-based ADCP data for the period March 1997 to December 2012 (Takikawa et al. 2005; Fukudome et al. 2010; Han et al. 2016) to compare with the HYCOM results.

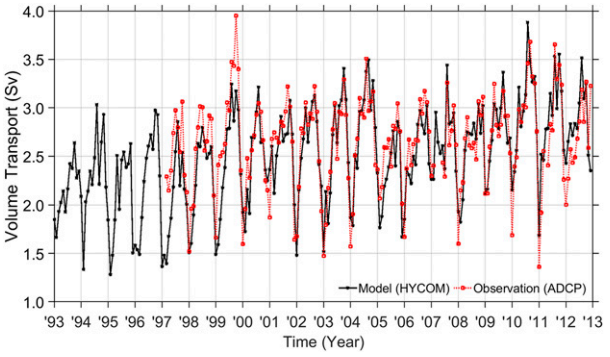

FIG. 2. Time series of monthly mean volume transport through Korea–Tsushima Strait (KS; positive into ES) from the model (black solid line, HYCOM reanalysis, 1993–2012) and observation (red dotted line, ADCP, 1997–2012).

In addition, cross-sectional structures of water temperature and the temporal difference observed during serial hydrographic cruises along one of the zonal lines (37.90°N) off the east coast of South Korea were compared with those given by HYCOM. We compared the deep-moored current-meter data collected at several depths ranging from 1800 to 2600 m in the JB, UB, and YB between 1993 and 2012 and those ranging from 2000 to 2400 m in the UB (Takematsu et al. 1999; Chang et al. 2002; Senjyu et al. 2005; Teague et al. 2005; Chang et al. 2009) with corresponding HYCOM mean currents. We averaged the EC1 moored current data from November 1996 to December 2012, which were recorded at 1400- and 2200-m depths using single-depth current meters attached to the subsurface mooring (Chang et al. 2009) and we compared these data with the HYCOM meridional currents in the western trough of the Ulleung Interplain Gap (UIG) between UI and DI (Fig. 1).

b. Methods

Zonal and meridional Ekman transports per unit width, within the surface Ekman layer (VT_{Ek_X} and VT_{Ek_Y}; $m^2\,s^{-1}$), were calculated from the meridional and zonal surface wind stresses using $VT_{Ek\_X} = (\tau_y/f\rho_0)$, $VT_{Ek\_Y} = (-\tau_x/f\rho_0)$, where τ_x ($N\,m^{-2}$), τ_y ($N\,m^{-2}$), $f = 2\Omega\sin\varphi$, Ω ($\approx 7.2921 \times 10^{-5}$ rad s^{-1}), φ, and ρ_0 ($\approx 1025\,kg\,m^{-3}$) denote the zonal and meridional wind stress, local Coriolis parameter, constant Earth rotation rate, latitude, and constant surface water density, respectively.

We estimated the meridional overturning streamfunction Ψ by zonally and vertically integrating the meridional current in units of Sverdrups ($1\,Sv = 10^6\,m^3\,s^{-1}$) (Cunningham and Marsh 2010; Kamenkovich and Radko 2011; Han et al. 2013), such that

$$\Psi(y,z,t) = \int_{z_{bot}(y)}^{z}\int_{x_e(y,z')}^{x_w(y,z')} v(x,y,z',t)\,dx\,dz'.$$

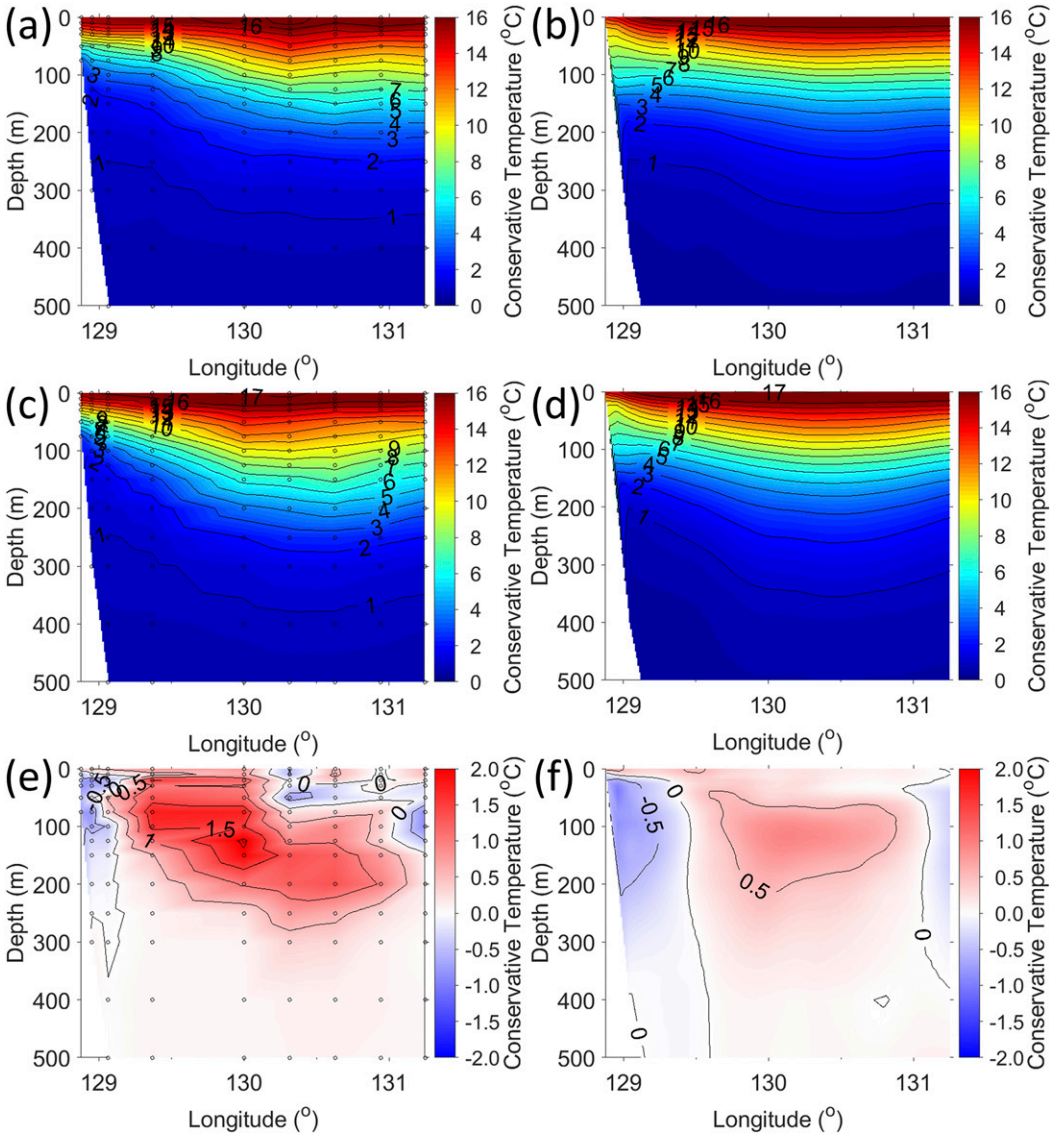

FIG. 3. Cross-sectional structures of temperature along zonal line at 37.90°N in the southwest ES (contour interval: 1°C) averaged (top) from 1997 to 1999 in Period I and (middle) from 2007 to 2009 in Period II, derived from (a),(c) serial hydrographic observations and (b),(d) HYCOM reanalysis. The differences are shown between the two periods from (e) observation [(c) − (a)] and (f) HYCOM [(d) − (b)].

Here, the meridional current v at longitude x, latitude y, depth z, and time t was integrated from the zonal easternmost point x_e to the westernmost point x_w, and from the bottom z_{bot} to the corresponding depth z.

The meridional overturning streamfunction Ψ was averaged over the total period (20 years) and the annual mean at a location of maximum temporal variance (1000 m, 38.48°N) was used as an ES MOC index. The years of negative (1996–2001 and 2010–12) and positive (1993, 2002, and 2004–09) phases of the ES MOC (when the ES MOC index exceeded one-third standard deviation of 0.26) were selected for composite analysis and grouped into Period I and Period II, respectively. The Ψ were averaged for the total 20-yr period to estimate the time mean structure and intensity of the ES MOC, and their seasonal climatology with a clear annual cycle. For example, the mean seasonal change in the ES MOC was determined from the climatological mean ES MOC structures for the four seasons (winter: DJF; spring: MAM; summer: JJA; and fall: SON). More important, the ES MOC structures during the two periods (Periods I and II) were determined from the composite based on the ES MOC index. The Ψ were averaged vertically over the two periods and the longitudinal difference was

compared at selected zonal sections along latitudes from 37° to 45°N in 1° increments, and at subsections covering deep troughs and shallow rises associated with the bathymetry, e.g., UB, JB, YB, Yamato Ridge (YR), and their connections (Fig. 1).

Horizontal currents (u, v), where u and v denote the zonal and meridional components, respectively, were averaged over the two periods (I and II) and spatially over cross sections of straits and selected zonal sections to allow a comparison of the ES MOC structures and associated volume transports. The horizontal currents at two different layers (intermediate and deep abyssal) were compared, where the intermediate and deep abyssal layers were defined as depths of 300–1500 m and below 1500 m, respectively. The reason for choosing these layers is to consider the shallow (~300 m) and deep (~1500 m) salinity minima and reported vertical boundaries of water masses, namely, ESIW, NKCW, CW, DW, and BW (Talley et al. 2003; Kim et al. 2004; Yoon et al. 2018). Note that the ESIW, NKCW, and CW primarily occupy the intermediate layer, whereas DW and BW occupy the deep abyssal layer.

3. Results

a. Validation of HYCOM

The net meridional volume transport V_{mod} (Sv) at 35°N across the KS calculated from the HYCOM meridional current was validated against the net volume transport observed using the ferry-based ADCP (i.e., V_{obs}). The mean values and standard deviations of V_{mod} and V_{obs} over 190 months (March 1997–December 2012) were consistent with each other at 2.59 ± 0.48 and 2.65 ± 0.47 Sv, respectively, yielding a significantly high (0.84) cross-correlation coefficient (black solid versus red dashed lines in Fig. 2). The difference (V_{mod} minus V_{obs}) had a time mean and standard deviation of −0.06 and 0.27 Sv, small enough compared with V_{mod} or V_{obs}, indicating that HYCOM effectively reproduced the net volume transport or inflow into the ES through the KS.

The cross-sectional structures of the water temperature averaged for the period January 1997–December 1999 (corresponding to Period I) and January 2007–December 2009 (corresponding to Period II) given by HYCOM and obtained through serial hydrographic observations were consistent (although not highly correlated quantitatively). In particular, the temperature difference between two periods (late 2000s minus late 1990s) was also consistent, successfully reproducing shallower onshore and deeper offshore thermoclines during the late 1990s compared with the late 2000s (Fig. 3). HYCOM successfully reproduced two different water masses observed in this cross section: 1) cold

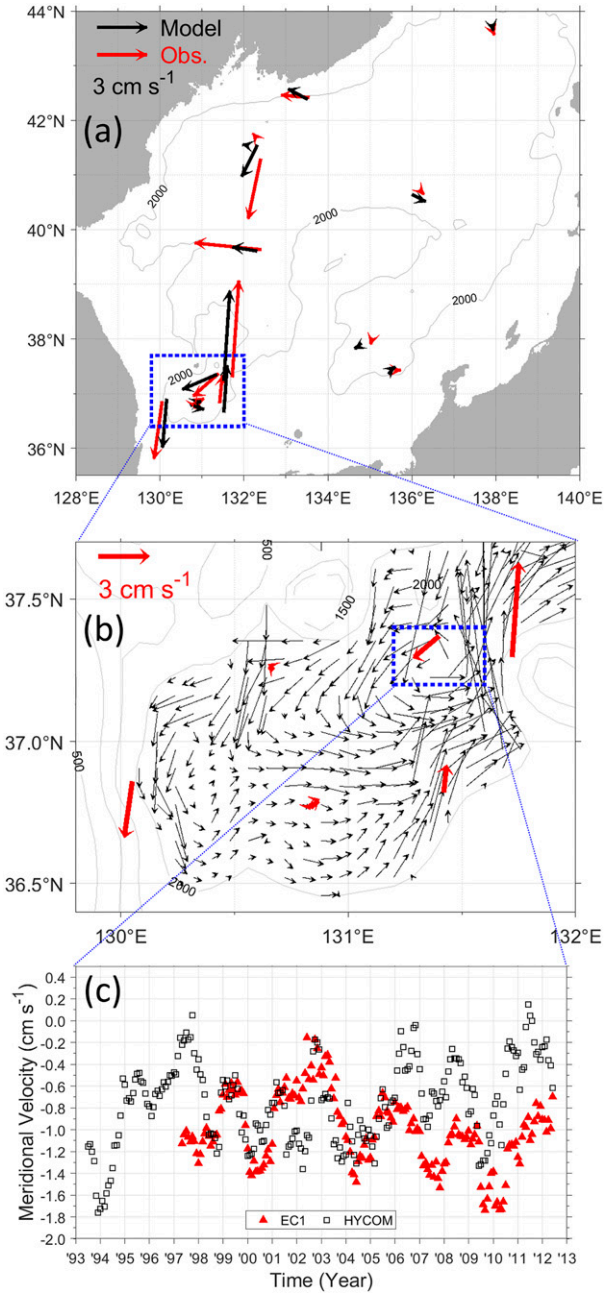

FIG. 4. Mean horizontal currents derived from HYCOM (black arrows) and moored current-meter observations (red arrows) averaged over depth ranging (a) from 1800 to 2600 m in the ES and (b) from 2000 to 2400 m in the UB [denoted by the dotted box in (a)]. The contour intervals for water depth in (a) and (b) are 2000 and 500 m, respectively. (c) The time series of meridional current derived from HYCOM (black squares) and observed at EC1 (red triangles).

(<5°C) and fresh (Absolute Salinity < 34.22 g kg^{-1}) water located below the thermocline, and 2) warm (>10°C) and saline (Absolute Salinity > 34.30 g kg^{-1}) water occupying the area between the onshore and

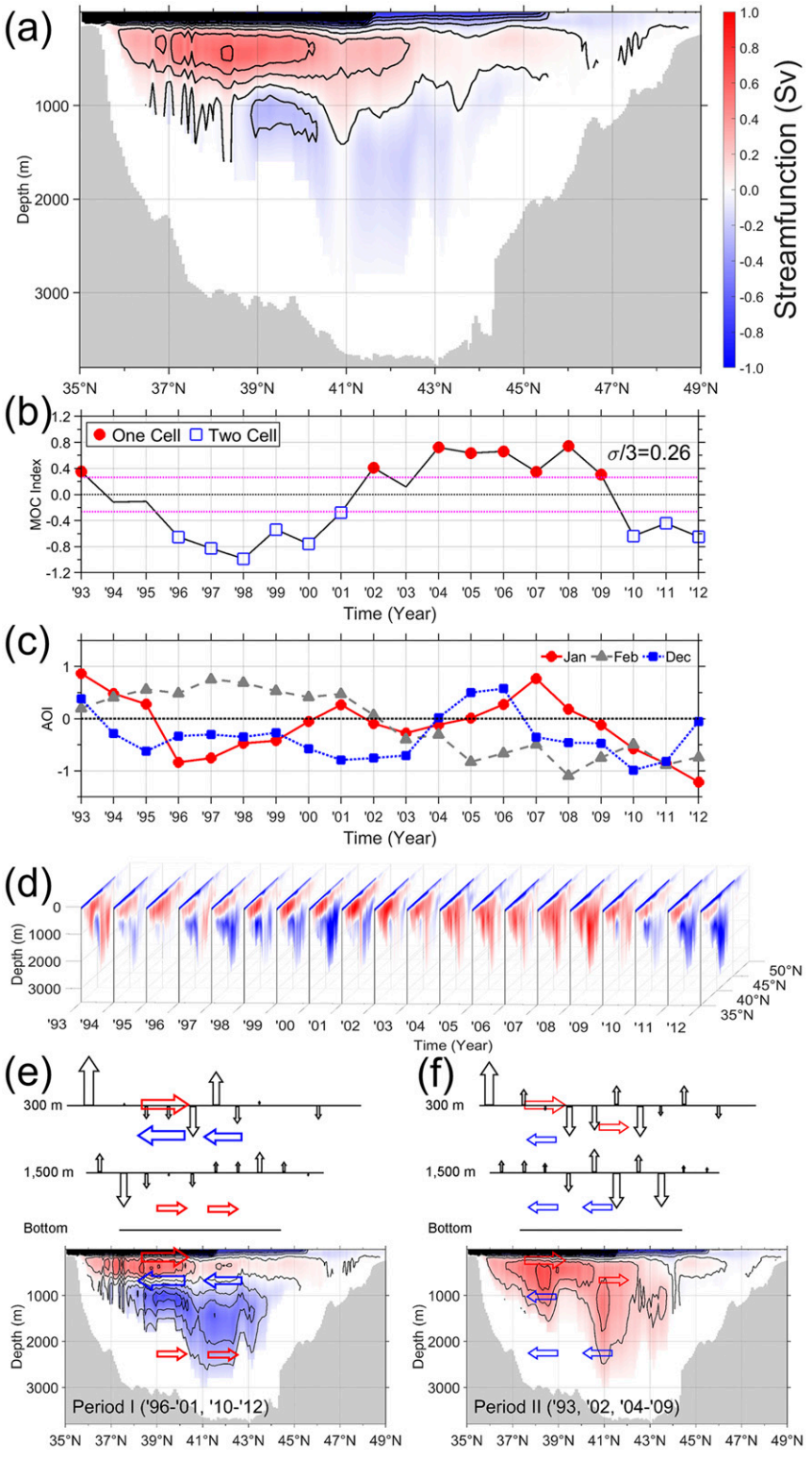

FIG. 5. (a) 20-yr (1993–2012) mean meridional overturning streamfunction representing the ES MOC structures, as derived from HYCOM reanalysis. (b) ES MOC index from annual mean meridional overturning streamfunction at 1000 m and 38.48°N. Years of positive (1993, 2002, and 2004–09, red filled circle) and negative (1996–2001 and 2010–12, blue open square)

offshore and around the thermocline. The former is known as the ESIW and is transported southward by the NKCC along the western boundary slope off the Korean Peninsula. The latter corresponds to the TWW, which is transported into the ES through the KS and advected northward by the western branch of the Tsushima Current or the East Korea Warm Current (EKWC) near the western boundary (east coast of the Korean Peninsula).

More interestingly, deep (~2000 m) horizontal currents in the JB, YB, and UB derived from the HYCOM (black arrows in Figs. 4a,b) agreed with the subsurface mooring measurements that have been reported previously (red arrows in Figs. 4a,b; Takematsu et al. 1999; Chang et al. 2002; Senjyu et al. 2005; Teague et al. 2005; Chang et al. 2009). That is, the HYCOM results conformed to general cyclonic circulation in the basins at the deep and abyssal layer, as derived from observations from 1993 to 1996 (Takematsu et al. 1999), from 1999 to 2000 (Chang et al. 2002), from 1999 to 2000 (Senjyu et al. 2005), from 1999 to 2001 (Teague et al. 2005), and from 2002 to 2004 (Chang et al. 2009). The decadal change in the deep abyssal (~2000 m) currents averaged over the western UIG (deep and abyssal inflow from JB into the UB, Fig. 4b) derived from the HYCOM generally conformed to the values obtained by the subsurface mooring EC1 observations, indicating a slight intensification of the southward inflow into the UB (Fig. 4c).

b. Streamfunction

In the meridional section of the 20-yr mean Ψ, anticyclonic overturning circulation occurred with $\Psi > 0$ (up- and downwelling in the south and north, respectively) at depths of <700 m (upper layer), along with cyclonic overturning circulation with $\Psi < 0$ (down- and upwelling in the south and north, respectively) at depths > 700 m (lower layer) (Fig. 5a). The minimum of the 20-yr average Ψ for the lower layer was −0.29 Sv at 1000 m and 39.28°N, whereas the maximum for the upper layer was 0.64 Sv at 400 m and 38.40°N. The two-cell MOC structure was maintained over seasons despite significant seasonal variations. The seasonal Ψ climatology (DJF, MAM, JJA, and SON) indicated that the minima in the lower layer were at 1100 m with time-varying amplitude and latitude, yielding −0.19 Sv at 38.96°N, −0.45 Sv at 40.16°N, −0.29 Sv at 39.84°N, and −0.40 Sv at 38.96°N for DJF, MAM, JJA, and SON, respectively (not shown). The maxima in the upper layer were 0.71 Sv at 500 m and 38.40°N, 0.64 Sv at 350 m and 37.44°N, 0.58 Sv at 400 m and 38.32°N, and 0.68 Sv at 400 m and 38.40°N in DJF, MAM, JJA, and SON, respectively. The northward flow (meridional volume transport) in the lower layer was largest (0.45 Sv) in MAM and smallest (0.19 Sv) in DJF, and the net southward flow (meridional volume transport) in the upper layer was largest (0.71 Sv) in DJF and smallest (0.58 Sv) in JJA. Despite the significant changes in the locations of the maximum and minimum Ψ over the seasons, the basic structure of the 20-yr mean ES MOC was maintained with the two counterrotating cells.

However, a fundamental change occurred in the ES MOC between Periods I (negative phase of ES MOC index including the late 1990s) and II (positive phase of ES MOC index including the 2000s), as revealed by a comparison of the corresponding Ψ structures (Figs. 5d–f). During Period I, the two counterrotating cells were intensified, with an anticyclonic shallow overturning circulation at depths < 700 m (upper cell) and a cyclonic deep overturning circulation at depths > 700 m (lower cell). In contrast, during Period II, anticyclonic overturning circulation prevailed at all depths and latitudes, yielding $\Psi > 0$ everywhere. One maximum Ψ value of +0.70 Sv at 400 m and 38.40°N was found, in addition to double-minimum Ψ values of −0.73 Sv at 1100 m and 39.84°N and −0.60 Sv at 1400 m and 41.52°N in the upper and lower layers during Period I (Fig. 5e). During Period II, double-maximum Ψ values of +0.72 Sv at 500 m and 38.16°N and +0.51 Sv at 1200 m and 40.88°N were found in both layers (Fig. 5f).

c. Horizontal circulation

The following significant changes occurred between Periods I and II in the horizontal circulation in the intermediate layer (300–1500 m):

1) A stronger southward current along the western boundary slope off the Korean Peninsula during Period I, i.e., the NKCC, which transports the ESIW

←

phases of the ES MOC are classified as ES MOC index exceeds one-third standard deviation of 0.26 (magenta lines). (c) 5-yr moving-averaged AO index in January (solid red circle), February (dashed gray triangle), and December (dotted blue square). (d) Time series of annual mean meridional overturning streamfunctions from 1993 to 2012. (e) 9-yr (1996–2001, 2010–12) and (f) 8-yr (1993, 2002, 2004–09) mean meridional overturning streamfunctions in Periods I and II, respectively. In (e) and (f), the zonally integrated meridional transports are denoted by horizontal arrows, and upwelling/downwelling at two depths of 300 and 1500 m are marked with vertical arrows, with the sizes of the latter being proportional to the volume transport. In (a), (e), and (f), the contour interval is 0.2 Sv.

(or NKCW) southward from the northwestern to southwestern ES, with amplitudes of the southward current (three blue rectangles off the Korean Peninsula in Figs. 6a,b) being 1.70, 2.41, and 2.86 cm s^{-1} during Period I versus 0.49, 0.50, and 0.24 cm s^{-1} during Period II.

2) A stronger northward current along the Russian coast during Period I, with amplitudes of the northward current (three red rectangles off the Russian coast in Figs. 6a,b) being 0.93, 1.35, and 1.85 cm s^{-1} during Period I versus 0.20, 0.93, and 0.46 cm s^{-1} during Period II.
3) Weaker anticyclonic circulation in the YB during Period I, with amplitudes of the vertical relative vorticity (red rectangle in the YB in Figs. 6a,b) being 3.91×10^{-5} s^{-1} during Period I versus 3.37×10^{-4} s^{-1} during Period II).
4) An opposite (cyclonic and anticyclonic circulations during Periods I and II) circulation in the UB (blue rectangle in the UB in Figs. 6a,b). The most striking feature is that the strong southward-flowing NKCC along the western boundary slope in the intermediate layer during Period I, which roughly followed a 1000-m isodepth horizontally, was not clear during Period II. This change was connected with markedly weakened or absent zonally integrated southward transport at the intermediate layer during Period II compared with Period I (Figs. 5e,f).

In addition, we found differences in the horizontal circulation between Periods I and II in the deep abyssal layer (>1500 m). That is, there were stronger cyclonic circulations in 1) JB, 2) UB, and 3) YB (blue rectangles in Figs. 6c,d), and 4) stronger northward deep abyssal currents in the eastern UIG (previously called the Dokdo Abyssal Current or DAC) and along the eastern slope of the YB (named here the East Yamato Basin Abyssal Current or EYBAC) during Period I (red rectangles in Fig. 6c). The amplitudes of the vertical relative vorticity in the JB, UB, and YB were 8.47×10^{-4}, 8.67×10^{-4}, and 1.021×10^{-3} s^{-1}, respectively, during Period I versus 4.43×10^{-4}, 5.09×10^{-4}, and 5.14×10^{-4} s^{-1}, respectively, during Period II (blue rectangles in Figs. 6c,d). The northward-flowing DAC and EYBAC were stronger during Period I (5.43 and 3.37 cm s^{-1}) than during Period II (2.66 and 1.50 cm s^{-1}). These strong cyclonic circulations within the basins and the stronger northward currents along the eastern slope of the basins in the deep abyssal layer during Period I were much weakened during Period II.

d. *Net meridional and vertical volume transports*

The net meridional volume transport in the intermediate layer was southward (negative) at all latitudes from 37° to 45°N during Period I and at latitudes 37°–40°N, 42°N, and 44°–45°N during Period II (Table 1). We found a significant decrease in amplitude or northward shift of the southward (negative) transport at the intermediate layer by 0.21–0.80 Sv from the difference during the two periods at latitudes 38°–44°N (bold in Table 1). In contrast to this northward (positive) shift of meridional transport in the intermediate layer, there was a significant southward (negative) shift of meridional transport in the deep abyssal layer at latitudes 38°–43°N from Period I to II (bold in Table 2). The northward versus southward shifts of the meridional transport in the intermediate versus deep abyssal layers during the two periods were consistent with the change caused by the two counterrotating MOC cells during Period I to one MOC cell during Period II (Fig. 5e versus Fig. 5f).

Spatially coherent northward (southward) shifts of the intermediate (deep abyssal) transport from Period I to II, e.g., late 1990s versus 2000s, were confirmed from those across the zonal subsections. In the intermediate layer, the meridional transport was generally negative (southward) at both the western and eastern subsections and positive (northward) in the central subsections, regardless of the period (Figs. 7a,b). However, strong southward transport, with amplitudes ranging from 0.39 to 0.76 Sv in the western subsections (off the Korean Peninsula) during Period I, were found to be weakened significantly during Period II, having a typical amplitude equal to or less than 0.14 Sv. In contrast, those in the eastern subsections, and particularly the northeastern part or eastern JB, converted from southward during Period I to northward in Period II (Figs. 7a,b). In addition, the down- and upwelling at 1500 m in the southern (i.e., 37°–41°N) and northern (i.e., 41°–45°N) subsections, respectively, during Period I were weakened or reversed during Period II, except 42°–43°N (symbols in Figs. 7c,d). Most interestingly, southward shifts of the deep abyssal transport were found from increased southward transports or reversed transports, i.e., at 38°N, from −0.03 to −0.18 Sv across the subsection connecting JB and UB; 39°N, from −0.03 to −0.22 Sv across the subsection connecting JB and UB, and from +0.38 to −0.08 Sv across the subsection connecting JB and YB; and 40°N, from +0.35 to −0.03 Sv and from +0.06 to −0.20 Sv (Figs. 5e,f and 7c,d).

Such contrasting northward and southward shifts of the meridional transport at the intermediate and deep abyssal layers from Period I to II were apparent from the annual time series of the 3-yr moving-averaged winter (JF) net meridional volume transport across the zonal section at 39°N, e.g., late 1990s versus 2000s (shaded areas in Fig. 8a). The winter net meridional transport across the zonal section at the intermediate layer

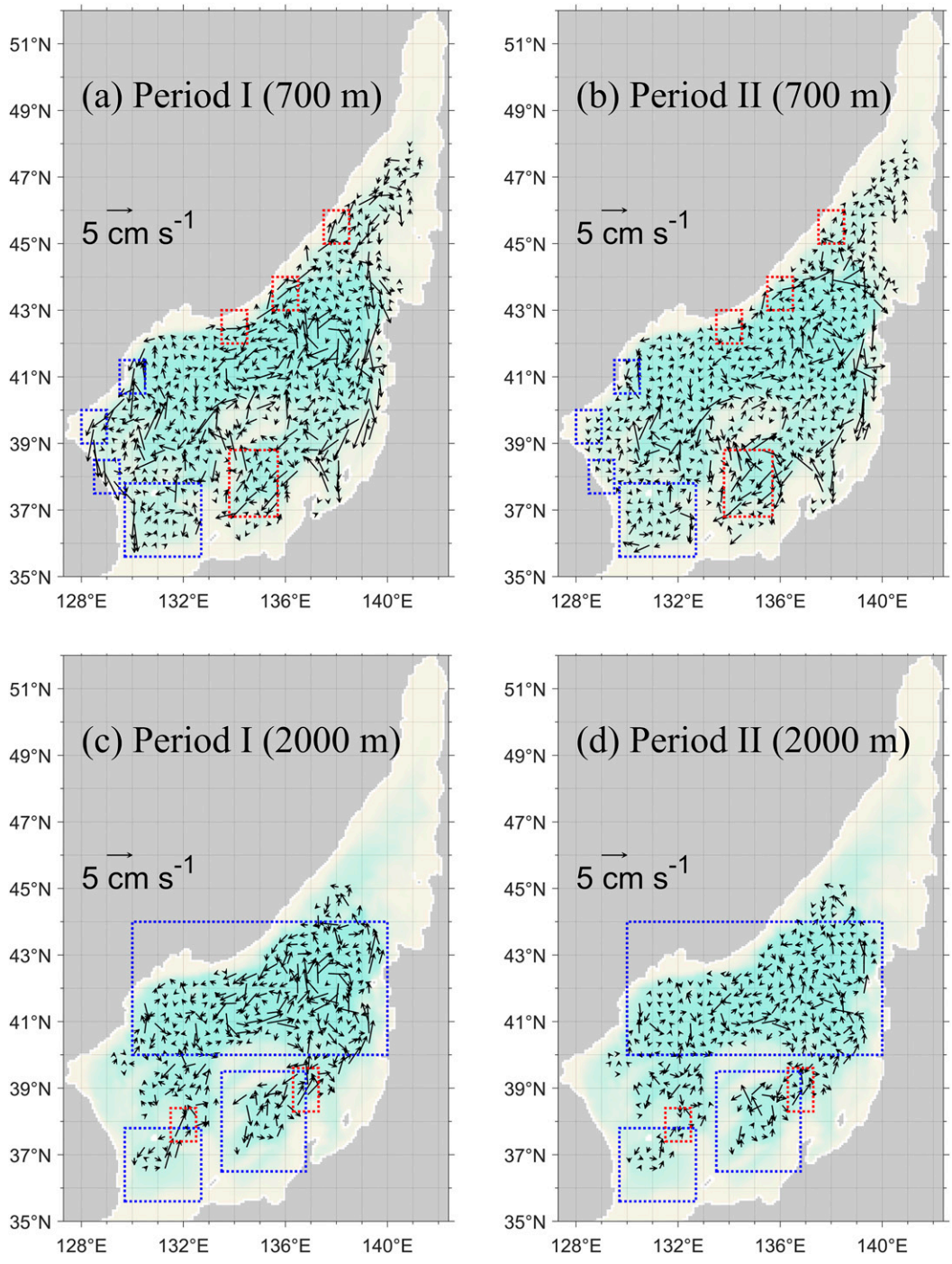

FIG. 6. Horizontal currents given by HYCOM at (a),(b) intermediate layer (700 m) and (c),(d) deep abyssal layer (2000 m), averaged over (left) Period I and (right) Period II. In (a) and (b), three sequential small blue and red dotted boxes represent the boundary current regions, and large blue and red boxes are UB and YB. Blue dotted boxes represent JB, UB, and YB anticlockwise from the top, and small red boxes are deep abyssal currents such as DAC (left box) and EYBAC (right box) in (c) and (d). The pale green background bathymetry is identical to that of Fig. 1.

TABLE 1. Net meridional volume transport in the intermediate layer (300–1500 m) averaged over Periods I and II, and their differences (Period II − Period I) at 37°–45°N. Negative (southward) values are in italics, and values in bold represent significant northward shifts from Period I to II.

Latitude	Transport (Sv, Period I)	Transport (Sv, Period II)	Difference (Period II − Period I)
45°N	*−0.14*	*−0.20*	*−0.06*
44°N	*−0.25*	*−0.04*	**+0.21**
43°N	*−0.45*	+0.24	**+0.69**
42°N	*−0.78*	*−0.28*	**+0.50**
41°N	*−0.49*	+0.31	**+0.80**
40°N	*−0.70*	*−0.18*	**+0.52**
39°N	*−0.82*	*−0.30*	**+0.52**
38°N	*−0.80*	*−0.44*	**+0.36**
37°N	*−0.39*	*−0.40*	*−0.01*

TABLE 2. As in Table 1, but the data are for the deep abyssal layer (>1500 m). Positive (northward) values are in italics, and values in bold represent significant southward shifts from Period I to II.

Latitude	Transport (Sv, Period I)	Transport (Sv, Period II)	Difference (Period II − Period I)
45°N	−0.02	*+0.04*	*+0.06*
44°N	*+0.09*	*+0.13*	*+0.04*
43°N	*+0.33*	−0.28	**−0.61**
42°N	*+0.45*	−0.08	**−0.53**
41°N	*+0.56*	−0.51	**−1.07**
40°N	*+0.40*	−0.23	**−0.63**
39°N	*+0.37*	−0.30	**−0.67**
38°N	*+0.21*	−0.21	**−0.42**
37°N	−0.20	−0.13	*+0.07*

remained southward, with only the amplitude decreasing from 1.03 Sv during the late 1990s (blue shaded) to 0.31 Sv during the 2000s (red shaded). However, the signs of those in the deep abyssal layer changed from positive (northward) to negative (southward) during the same period (Fig. 8a).

4. Discussion

The results of this study presented in the previous section indicated a considerable change in the ES MOC from the 20-yr mean structure with two counterrotating cells, consistent with the 40-yr mean ES MOC reported previously (Park et al. 2013). The shallow and deep overturning circulations were intensified in the intermediate and deep abyssal layers during the late 1990s (Period I), yielding the counterrotating two-cell structure that is closer to the 20-yr mean ES MOC structure. Subsequently, the two-cell structure changed significantly to become a single full-depth overturning cell during the 2000s (Period II), which lasted to before the early 2010s, when it reverted to the two-cell structure. We noted that the intermediate and deep abyssal layers at 300–1500 m and below 1500 m, respectively, correspond to the shallow and deep salinity minima and known water boundaries (Kim and Chung 1984; Kim and Kim 1999; Kim et al. 2004; Talley et al. 2006; Chang et al. 2016; Nam et al. 2016; Yoon et al. 2018). This decadal change in ES MOC accompanied contrasting northward and southward shifts in the net meridional volume transport at the intermediate and deep abyssal layers from the late 1990s (Period I) to the 2000s (Period II), respectively. Although such decadal ES MOC changes have not been examined previously, a number of publications, discussed below, provide further support to our findings.

a. Intermediate layer (300–1500 m)

Despite known difficulty in numerically reproducing the shallow salinity minimum in the southwestern ES (salinity minimum in the intermediate layer), HYCOM could successfully reproduce the shallow convection of the low-salinity intermediate water, i.e., ESIW, which has long been recognized from hydrographic observations (Kim and Chung 1984; Kim and Yoon 1999; Kim and Kim 1999; Kim et al. 2004; Talley et al. 2006). In addition, HYCOM could reasonably simulate realistic intermediate circulation in the southwestern ES, yielding, e.g., decadal changes of ESIW properties associated with the AO (Cui and Senjyu 2010; Tanaka 2014; Nam et al. 2016). The formation, properties, volume, and distribution of the ESIW vary from year to year and over the decades, being influenced by the upper 500-m ocean circulation in the ES, as well as atmospheric forcing linked to AO (Kim et al. 2004; Teague et al. 2005; Chang et al. 2016; Nam et al. 2016; Park and Nam 2018). This influence is particularly prominent in the western ES, where water formation processes, such as subduction and the footprint of shallow convection in the northwestern ES (area A in Fig. 1) have been reported (Chang et al. 2016; Nam et al. 2016; Park and Lim 2017). These likely had a major impact on the southward western boundary current at the intermediate layer, i.e., NKCC, off the Korean Peninsula and, therefore, the ES MOC. The cyclonic horizontal circulations in the intermediate layer reproduced by HYCOM, particularly during Period I (Fig. 6a), are consistent with the observations made using Argo float trajectories between 1999 and 2010 (e.g., Fig. 5 of Park et al. 2013) and intermediate circulations derived from Argo float trajectories between 1998 and 2004 in the southwestern ES [e.g., Fig. 4 of Park et al. (2004) and Fig. 3 of Park et al. (2010)]. Here, we discuss the results of ES MOC in relation to internal ES circulation at the intermediate

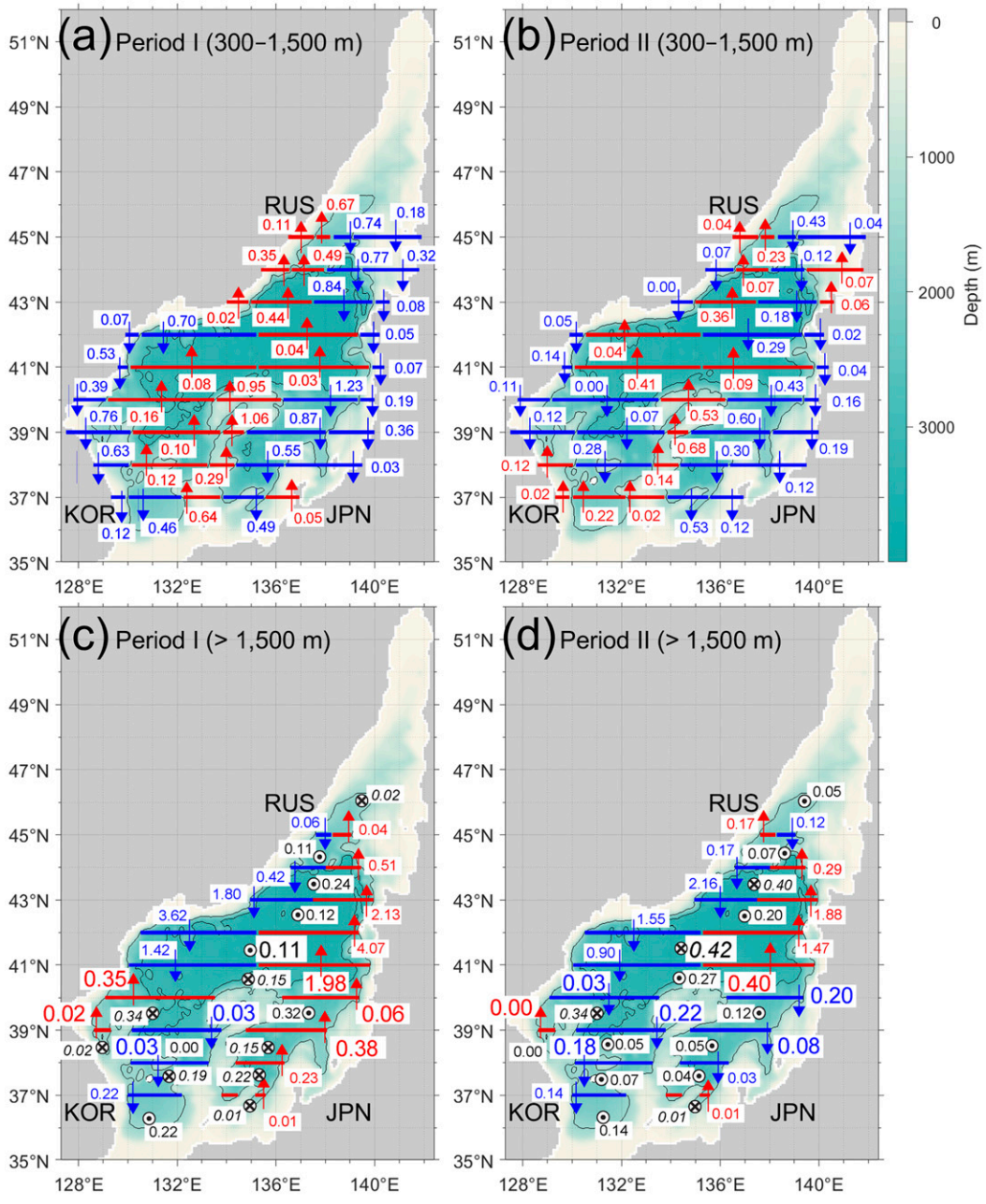

FIG. 7. Schematics of meridional circulation (volume transport) in (a),(b) intermediate (300–1500 m), and (c),(d) deep abyssal (below 1500 m) layers in (left) Period I and (right) Period II. Red (blue) arrows represent northward (southward) transport, and black arrowhead (arrow tail) symbols with normal (italic) numbers denote upwelling (downwelling) at layer top at 1500 m, respectively. The numbers indicate the net meridional volume transport in units of Sverdrups.

layer and air–sea fluxes of heat, freshwater, buoyancy, and momentum.

The two-cell MOC structures during Period I imply enhanced shallow convection and more active ESIW formation in the northwestern ES (area A) than in Period II, or, in other words, the ESIW formation was likely less active during Period II (Figs. 5e,f). Area A (centered at 130°E, 41.25°N) falls within an area where the sea surface salinity and depth of the salinity minimum layer reach their minima where the ESIW is formed (see Fig. 3 of Park and Lim 2017). In the early 2000s, the sea surface temperature and salinity averaged over area A increased significantly by 0.76°C (from 4.10°C in the late 1990s to 4.86°C in the 2000s) and

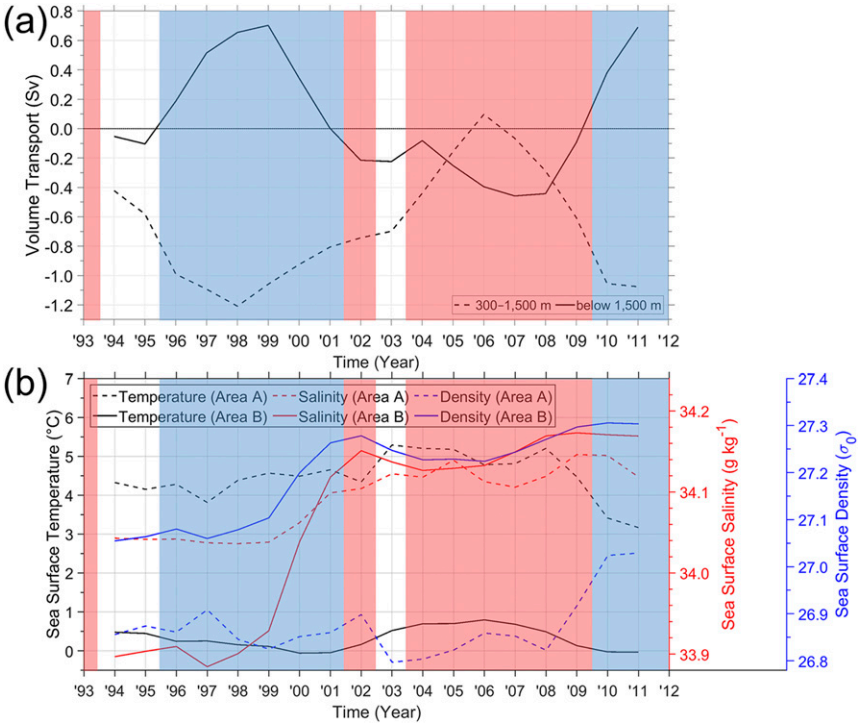

FIG. 8. (a) Annual time series of 3-yr moving-averaged winter (JF) net meridional volume transport (Sv; positive northward) across zonal section at 39°N in the intermediate layer (between 300 and 1500 m; black dashed) and deep abyssal layer (below 1500 m; black solid) from 1994 to 2011. (b) Annual time series of 3-yr moving-averaged winter (JF) mean sea surface Conservative Temperature (°C; black), sea surface Absolute Salinity (g kg^{-1}; red), and sea surface potential density (in σ_0; blue) from 1994 to 2011, averaged over areas A (dashed lines) and B (solid lines) of Fig. 1. Those in Periods I and II are shaded with light blue and red colors, respectively.

0.05 g kg^{-1} (from 34.07 g kg^{-1} in the late 1990s to 34.12 g kg^{-1} in the 2000s), respectively, yielding a sea surface density decrease of 0.05 kg m^{-3} (in σ_0) for the decade from the late 1990s to the 2000s (Fig. 8b).

Such decrease in surface density could be induced by either buoyancy gain from the atmosphere or changes in wind-driven upper-ocean circulation or both. Cross-isopycnal mass flux estimated using the method used in Speer and Tziperman (1992) supported more active formation of the intermediate water (density ranging from 27.0 to 27.4 kg m^{-3}) in area A during Period I than during Period II. This indicates higher transformation primarily because of higher isothermal (rather than isohaline) volume flux and the larger surface area of water having a range of densities corresponding to the intermediate water (Figs. 9a,b). Indeed, the surface heat flux anomaly averaged over area A changed from a negative phase during Period I to a positive phase during Period II. This resulted in buoyancy gain and a consequent decrease in sea surface density in the late 2000s primarily because of surface heat gain during the 2000s (Figs. 9c and 10a). The increased heat gain from the atmosphere into the ocean during Period II compared with Period I could be seen in an area wider than area A, with contrasting surface heat flux anomalies over the entire basins during the two periods (Figs. 11a,b). In addition to the surface heat flux, surface momentum flux affected the low sea surface density during the 2000s compared with the late 1990s, showing the increase in northward Ekman transport (vertical bars in Fig. 10a) in the southwestern ES (UB, rectangles in Figs. 11g,h) because of stronger westward wind stress (or weaker eastward wind stress) (Figs. 11g,h). The northward transport anomaly of warm TWW to the northwestern ES during the 2000s favored higher sea surface temperature in the formation area (area A). Therefore, both air–sea buoyancy exchange and changes in wind-driven upper-ocean circulation were responsible for the conditions unfavorable to active subduction and ESIW formation during the 2000s. This resulted in enhanced stratification, with warmer and lower-density surface water overlying colder and higher-density intermediate water in area A (Fig. 9c).

The strong stratification in area A could stabilize the upper water column and reduce the ESIW formation

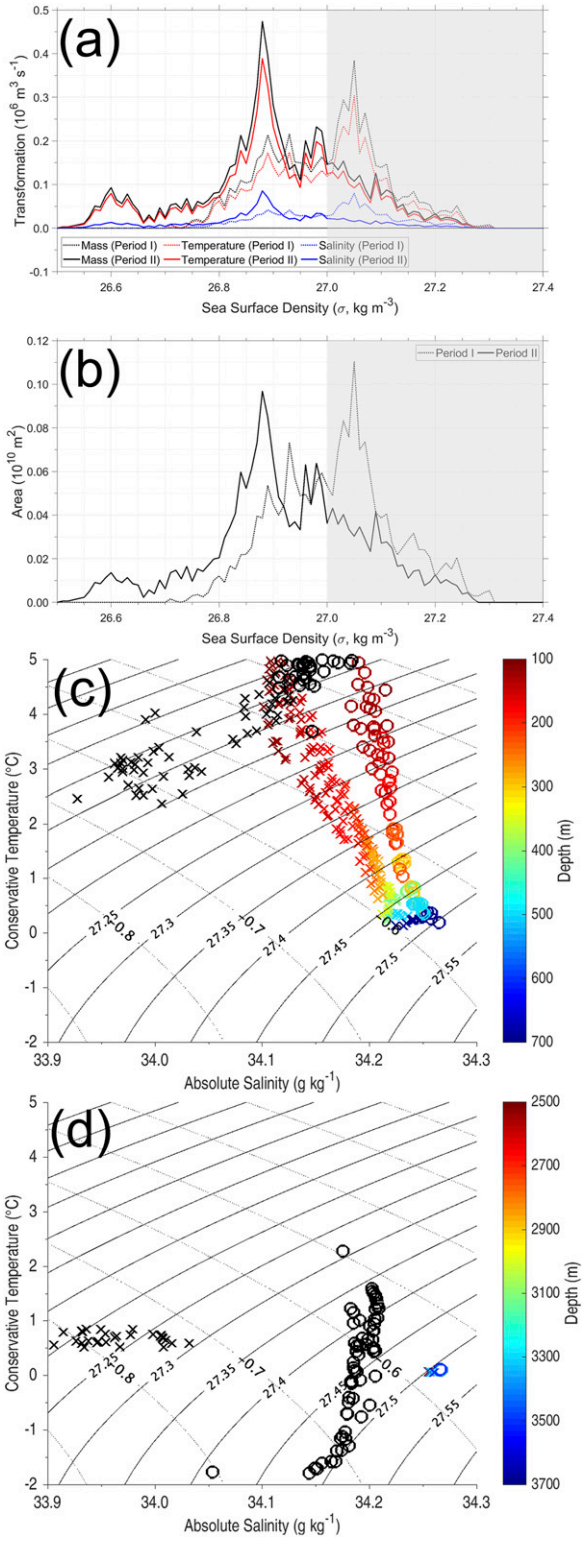

FIG. 9. (a) Cross-isopycnal mass flux (volume transport; m^3 s^{-1}) or transformation as a function of sea surface density (σ; kg m^{-3}) in area A in February (Speer and Tziperman 1992). Plot of transformation of total (mass; black), thermal (temperature; red), and haline (salinity; blue) fluxes for Periods I (dotted line; two-cell) and II (solid line; one-cell). (b) Areas of each density class (interval of σ is 0.01 kg m^{-3}) in area A in February are plotted for Periods I (dotted line; two-cell) and II (solid line; one-cell). The densities of intermediate water are shaded with light gray in (a) and (b). TS properties of (c) sea surface water (black symbols) in area A and intermediate water (between 100 and 700 m red to blue) in the area west of 128.72°E and at 39.00°N, and (d) sea surface water (black symbols) in area B and deep abyssal water (>2500 m, red to blue) in the JB for Period I (February 1998; "X" symbols) and Period II (February 2008; "O" symbols), derived from HYCOM.

during the 2000s (Period II), contrasting with active water transformation during the late 1990s (Period I). This behavior could also facilitate the weaker NKCC at the intermediate layer and northward shifts in the meridional transport at the layer during the 2000s (Fig. 6a versus Fig. 6b). This decreased the southward intermediate transport across 39°N significantly (0.72 Sv) from −1.03 Sv in the late 1990s to −0.31 Sv in the 2000s (dashed line in Fig. 8a). We noted that the NKCC transport at depths, particularly ranging from 300 to 700 m, near the western boundary decreased markedly by 0.62 Sv (from −0.69 Sv in the late 1990s to −0.07 Sv in the 2000s, not shown), which accounts for most changes in the meridional transport in the intermediate layer.

To date, no results identical to those obtained here have been reported for the decadal changes in ESIW formation in the northwestern ES. However, our findings are consistent with the water properties and transport and their temporal changes reported previously (Kim and Kim 1999; Kim et al. 2004; Cui and Senjyu 2010; Tanaka 2014; Nam et al. 2016). In particular, Nam et al. (2016) suggest that the ESIW properties, volume, and distribution are connected primarily to the winter atmospheric conditions off the Russian coast in the northern ES and AO index over the decadal time scale. The decadal shift in the ES MOC index from the late 1990s to the 2000s covaries with the January AO index (shift from negative to positive phase, Fig. 5c) among three winter AO indices (December, January, and February). This yielded correlation coefficients of 0.62 and 0.65 between the January AO index and the ES MOC index and between the January AO index and meridional intermediate transport, respectively. However, as also suggested by Nam et al. (2016), the upper-ocean circulation in the southwestern ES can play an important role in ESIW formation, properties, volume, and distribution at the interannual time scale. The greater EKWC transport and more volume of TWW transported into the northwestern ES by a weaker westerly wind (westward wind stress anomaly) in the UB combined with reduced ESIW formation

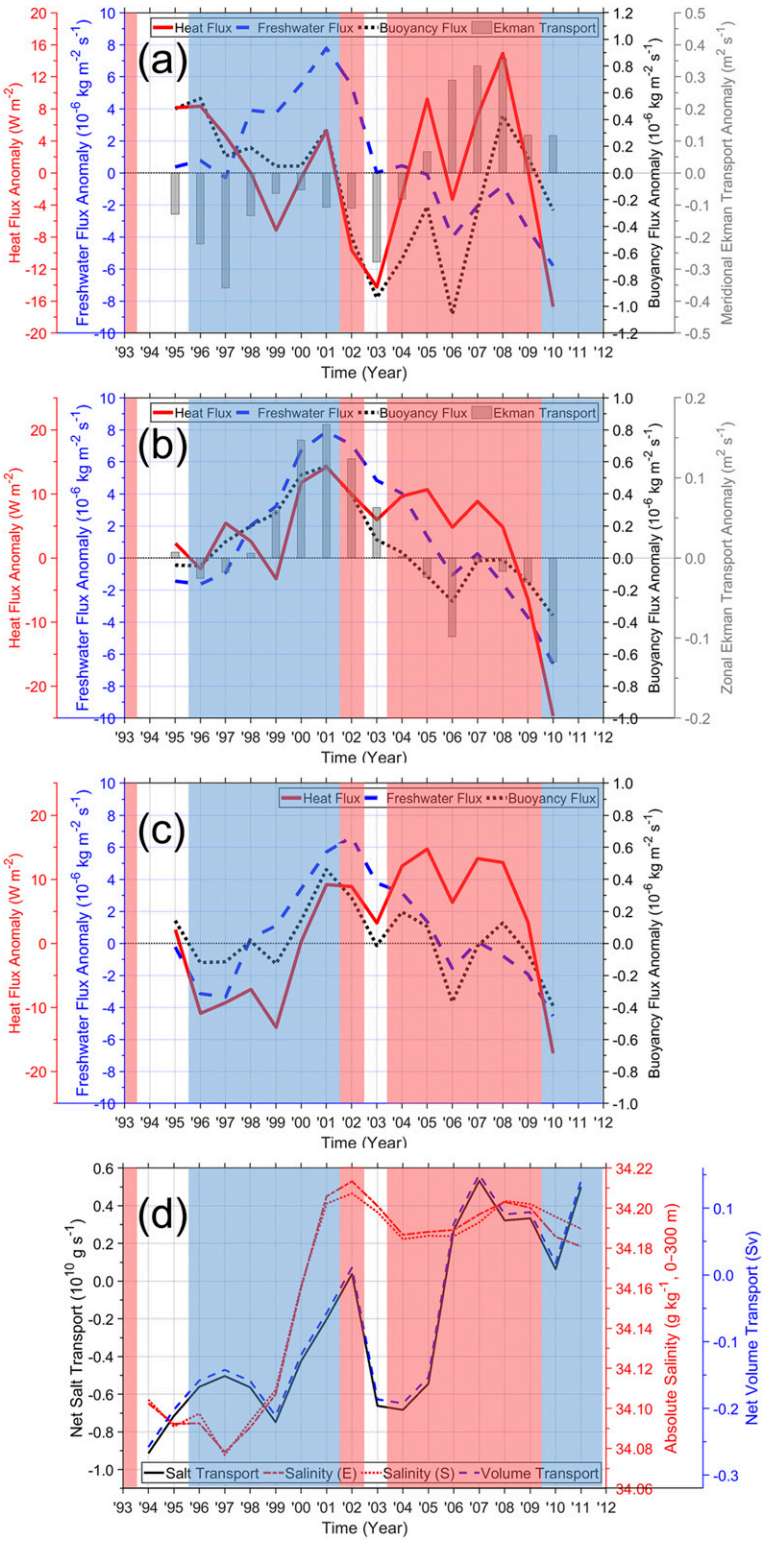

FIG. 10. Time series of 5-yr moving averaged January surface net heat flux anomaly [left y axis ($\mathrm{W\,m^{-2}}$); a positive sign represents heat gain from the atmosphere into the ocean, red solid line], surface freshwater flux anomaly [left y axis ($\mathrm{kg\,m^{-2}\,s^{-1}}$); precipitation minus evaporation, which means that a positive sign

could yield warmer (and more saline) ESIW, with reduced southward NKCC transport at the intermediate layer.

b. Deep abyssal layer (>1500 m)

As regards the deep abyssal layer, it has been reported that the ES is severely ventilated down to the bottom as a result of surface atmospheric and oceanic conditions off the Russian coast in the northern ES (particularly at area B, Fig. 1). This yields the highest levels of deep dissolved oxygen and lowest deep-water temperature in the Pacific (Kim et al. 2004; Talley et al. 2006). In particular, the BW has been suggested to be formed in area B during winter through deep-slope convection when the sea surface density (primarily salinity) increases because of brine rejection through sea ice formation, more evaporation minus precipitation, and more TWW transport into the formation area or area B (Noh and Jang 1999; Kang et al. 2003; Talley et al. 2003; Kim et al. 2004; Cui and Senjyu 2010; Yoon et al. 2018). Most recently, Yoon et al. (2018) have suggested that the formation of the deep water masses (CW, DW, and BW) and ventilation of the ES had experienced significant decadal changes in the early 2000s in relation to contrasting surface conditions off the Russian coast between the 1990s and 2000s. Such changes in deep ventilation could link to deep abyssal circulation and ES MOC, although these have not been reported despite several researchers suggesting dominant cyclonic abyssal circulations in JB, UB, and YB because of topographic control (Seung and Yoon 1995; Chang et al. 2002; Senjyu et al. 2005; Seung 2005; Yoon et al. 2005; Kim et al. 2008; Chang et al. 2016). Here, we discuss the results of decadal change in the ES MOC in relation to deep ventilation and deep abyssal circulation.

The ES MOC structures imply more BW formation through active deep-slope convection during Period II than during Period I in area B. The winter (JF) temperature, salinity, and density at the sea surface in area B increased by 0.07°C from 0.45° to 0.52°C, 0.14 g kg^{-1} from 34.01 to 34.15 g kg^{-1}, and 0.08 kg m^{-3} from 27.17 to 27.25 kg m^{-3}, respectively, during the early 2000s (Fig. 8b, solid lines). This increase in the sea surface density primarily because of salinity increase (Fig. 9d) is associated with both local atmospheric forcing and upper-ocean circulation. More loss of surface buoyancy from ocean to atmosphere was found because of more evaporation minus precipitation during Period II in area B (Figs. 10b,c and 11c,d). Therefore, the results indicated the importance of the regional air–sea freshwater (buoyancy) exchange on the BW formation, as also suggested previously (Kim et al. 2002; Talley et al. 2003; Yoon et al. 2018). Furthermore, horizontal salt convergence primarily because of volume convergence at the upper 300 m into area B increased from both the southern and the eastern cross sections by 0.88×10^7 kg s^{-1} (-0.56×10^7 kg s^{-1} in the late 1990s to 0.32×10^7 kg s^{-1} in the 2000s), further supporting the increase in sea surface salinity and density in area B (Fig. 10d). This increased horizontal salt convergence into area B is related closely to the recirculation of saline TWW partly driven by westward Ekman transport (vertical bars in Fig. 10b) because of the southward wind stress anomaly in the northeastern ES (rectangles in Figs. 11e,f).

These factors supported surface conditions that were favorable to more active deep-slope convection to activate the BW formation during Period II, yielding the sea surface density in area B as high (~27.5 kg m^{-3}) as that corresponding to the bottom water density (Fig. 9d). In turn, this facilitated the weaker northward abyssal currents along the eastern slope boundaries of the UB and YB (DAC and EYBAC, respectively) that occurred during the 2000s or Period II (Figs. 6c,d). Weaker northward abyssal currents linked to a southward shift from northward to southward transport over the decade from Period I to II were found in the deep abyssal layer across 39°N (Fig. 8a, solid line). This shift can be explained mainly by considering the weakening of the two northward abyssal currents (DAC and EYBAC) that occurred during Period II (Figs. 6c,d). The southward shift of the net meridional transport in the deep abyssal

←

represents freshwater gain from the atmosphere into the ocean, blue dashed line], and surface net buoyancy flux anomaly [right y axis (kg m^{-2} s^{-1}); a positive sign represents buoyancy gain from the atmosphere into the ocean, black dotted line] in areas (a) A, (b) B, and (c) C, respectively. In (a) and (b), superimposed are meridional and zonal Ekman transport anomalies per unit width in the southwestern and northeastern ES, respectively [right y axis (m^2 s^{-1}); a positive sign represents northward in (a) and eastward in (b), gray bar]. (d) Time series of 3-yr mean January and February (horizontal and vertical) net salt transport [left y axis (g s^{-1}); black solid line], salinity [right y axis (g kg^{-1})] at upper 300 m of eastern (red dash dotted line) and southern (red dotted line) boundaries of area B, and net volume convergence into area B [right y axis (Sv); blue dashed line]. Periods I and II are shaded by light blue and red colors, respectively.

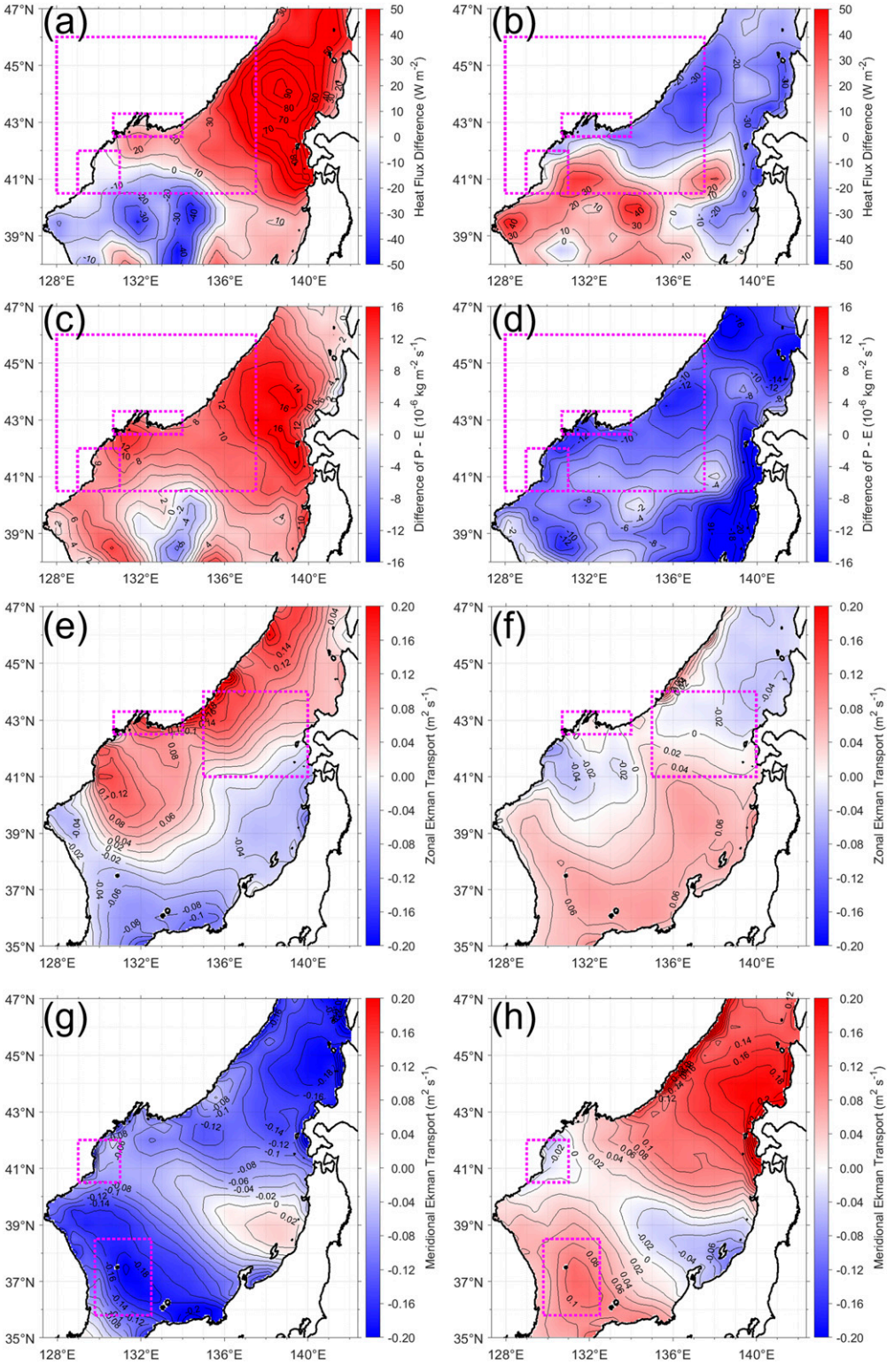

FIG. 11. Temporal differences in January mean (a),(b) surface net heat flux anomaly (W m^{-2}; a positive sign represents increase in heat gain from the atmosphere into the ocean) and (c),(d) surface freshwater flux anomaly (kg m^{-2} s^{-1}; precipitation minus evaporation, a positive sign represents increase in freshwater gain from the atmosphere into the ocean) for Period I in (a) and (c) and Period II in (b) and (d). January mean (e),(f) zonal and (g),(h) meridional Ekman transport anomalies per unit width [m^2 s^{-1}; a positive sign

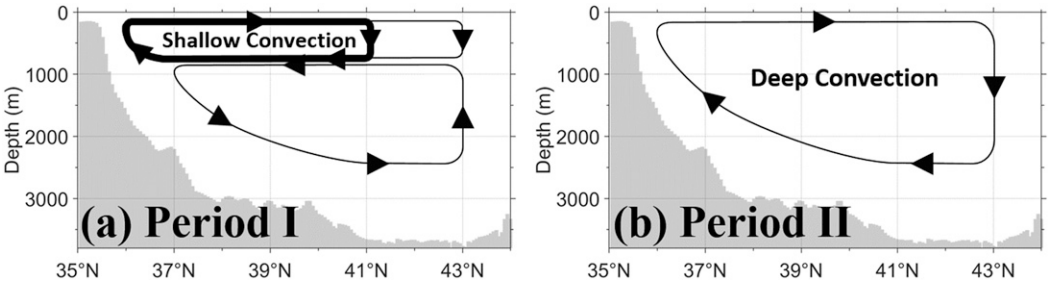

FIG. 12. Schematic of ES MOC for (a) shallow convection (subduction) in Period I (two-cell years, late 1990s) and (b) deep (slope) convection in Period II (one-cell years, 2000s).

layer contributed to the ES MOC shift from two (shallow and deep) counterrotating overturning cells during the late 1990s (Period I) to a single full-depth cell during the 2000s (Period II), along with the northward shift in the intermediate layer (Figs. 5e,f). The more active deep-slope convection and enhanced BW formation because of increased sea surface salinity and density in area B during the 2000s were consistent with the southward shift in deep abyssal transport and the weakened DAC and EYBAC.

These decadal changes in BW formation in the northern ES have not been fully addressed to date, but some features on abyssal circulation and decadal changes in BW formation are consistent with previous findings (Yoshikawa et al. 1999; Kang et al. 2003; Talley et al. 2003; Kim et al. 2004; Senjyu et al. 2005; Cui and Senjyu 2010; Yoon et al. 2018). Cyclonic abyssal circulations in JB, UB, and YB, previously derived from moored current-meter observations, are consistent with the findings of the present study (Takematsu et al. 1999; Chang et al. 2004; Senjyu et al. 2005; Teague et al. 2005; Yoon et al. 2018). We noted that a recent study by Yoon et al. (2018) came to similar conclusions with regard to the importance of both horizontal salt convergence at the upper ocean and air–sea freshwater exchange in modifying deep ES ventilation. Previous studies using hydrographic observations over the period 1969–96 and a moving-boundary box model revealed markedly weakened ES ventilation from BW to CW, with reduced BW formation through deep-slope convection and greater CW formation through open-ocean convection in the mid-1990s (Kim et al. 2004). However, by incorporating hydrographic data collected over the recent decade, Yoon et al. (2018) revealed a slowdown in the deepening of the DW–BW boundary since the 2000s, which is associated with the reinitiation of BW formation through deep-slope convection in area B. Finally, the important role of local air–sea freshwater flux and horizontal salt convergence into area B in relation to the reinitiation of BW formation in the 2000s were also highlighted by Yoon et al. (2018), consistent with the results in this study.

5. Summary and conclusions

We have shown significant decadal changes in the strength and structure of the ES MOC using the 20-yr HYCOM reanalysis data validated against in situ observations of 1) net volume transport across the KS, 2) zonal cross-sectional structures of the water temperature off the western boundary, 3) deep abyssal circulation patterns, and 4) decadal changes in the deep meridional currents flowing from JB into UB. The results of the zonally integrated meridional volume transport indicate a 20-yr-mean ES MOC structure having two counterrotating overturning cells that consist of shallow-anticyclonic and deep-cyclonic overturning circulations, with upwelling in the south and downwelling in the north at the intermediate layer and vice versa in the deep abyssal layer, respectively (Fig. 12). More interestingly, significant decadal shifts in the ES MOC were found to discern two-cell and one-cell years (Period I, late 1990s versus Period II, 2000s). That is, the ES MOC changed in the early 2000s from two counterrotating cells (late 1990s) to a single full-depth cell (2000s) associated with a weakened southward NKCC (northward shift in net meridional volume transport) in the intermediate layer and weakened northward DAC and EYBAC (southward shift in net meridional volume transport) in the deep

←

represents eastward in (e) and (f) and northward in (g) and (h)] for Period I in (e) and (g) and Period II in (f) and (h). Areas A, B, and C in (a)–(d), Area B and the area in the northeastern ES for Ekman transport time series shown in Fig. 10b in (e) and (f), and Area A and the area in the southwestern ES for Ekman transport time series shown in Fig. 10a in (g) and (h) are plotted with magenta lines.

abyssal layer (Fig. 12a versus Fig. 12b). Further analysis suggested that the weakening of southward-flowing NKCC (northward-flowing DAC and EYBAC) and the northward (southward) shift in the net meridional volume transport in the intermediate (deep abyssal) layer during Period II were driven primarily by reduced ESIW (more BW) formation, with increased sea surface temperature (increased sea surface salinity) in area A (area B) in the northwestern ES.

In conclusion, our results suggested that the ES MOC responded to both external atmospheric forcing and internal ES processes. The dominant internal forcing mechanism for the decadal ES MOC shift is wind-driven northward Ekman transport in the southwestern ES and horizontal salt convergence in the northwestern ES, associated with wind-driven westward Ekman transport and recirculation of TWW at the upper ocean in the northeastern ES. These factors provided a condition unfavorable to ESIW formation and favorable to BW formation during Period II. Such internal process could be enhanced further by water mass transformation and buoyancy gain (loss) from ocean to atmosphere at the surface in area A (area B) in the northwestern ES during Period II. This implies that area A (area B) was facilitated primarily by heat gain from (freshwater loss to) the atmosphere during Period II linked to the January AO. External forcing by the westward (southward) surface wind stress anomaly and the resultant northward (westward) anomaly in Ekman transport in the southwestern (northeastern) ES likely reinforced the upper-ocean convergence of warm and saline TWW in the northwestern ES.

In this study, we have shown that the ES MOC, horizontal recirculation of TWW, formations of intermediate and bottom waters in the northwestern ES, transport at the upper, intermediate, and deep abyssal layers in the ES, and air–sea fluxes of heat, freshwater, buoyancy, and momentum covary at a decadal time scale. However, our study did not allow determining which drives which, or whether other processes drive these. Given the importance of the ES MOC for transport of heat, salt, and volume, it is likely that feedback occurs between the external atmospheric forcing and internal circulation. Therefore, future numerical modeling study is necessary to address the feedback mechanisms, if any. Understanding how such feedbacks affect the decadal variability of the ES MOC has implications for the response of other marginal seas and the global ocean to future climate change.

Acknowledgments. The EC1 mooring data and serial hydrographic observation data are available at OceanSITES (http://www.oceansites.org)/SEANOE (http://doi.org/10.17882/58134) and via NIFS, Republic of Korea, respectively. We thank H. J. Lee and N. Hirose, who provided us with the ferry-mounted ADCP data. The 1/12° global HYCOM+NCODA Ocean Reanalysis was funded by the U.S. Navy and the Modeling and Simulation Coordination Office. Computer time was made available by the DoD High Performance Computing Modernization Program (http://hycom.org). The surface shortwave, longwave, sensible heat, and latent heat fluxes, evaporation, precipitation, and wind stress data were obtained from MERRA-2 (https://gmao.gsfc.nasa.gov/reanalysis/MERRA-2). This work was part of the project titled "Deep Water Circulation and Material Cycling in the East Sea" (20160040) funded by the Ministry of Oceans and Fisheries (MOF), Republic of Korea.

REFERENCES

Chang, K.-I., N. G. Hogg, M.-S. Suk, S.-K. Byun, Y.-G. Kim, and K. Kim, 2002: Mean flow and variability in the southwestern East Sea. *Deep-Sea Res. I*, **49**, 2261–2279, https://doi.org/10.1016/S0967-0637(02)00120-6.

——, and Coauthors, 2004: Circulation and currents in the southwestern East/Japan Sea: Overview and review. *Prog. Oceanogr.*, **61**, 105–156, https://doi.org/10.1016/j.pocean.2004.06.005.

——, K. Kim, Y.-B. Kim, W. J. Teague, J. C. Lee, and J.-H. Lee, 2009: Deep flow and transport through the Ulleung Interplain Gap in the southwestern East/Japan Sea. *Deep-Sea Res. I*, **56**, 61–72, https://doi.org/10.1016/j.dsr.2008.07.015.

——, C.-I. Zhang, C. Park, D.-J. Kang, S.-J. Ju, S.-H. Lee, and M. Wimbush, 2016: *Oceanography of the East Sea (Japan Sea)*. Springer, 460 pp.

Cho, Y. K., and K. Kim, 1998: Structure of the Korea strait bottom cold water and its seasonal variation in 1991. *Cont. Shelf Res.*, **18**, 791–804, https://doi.org/10.1016/S0278-4343(98)00013-2.

——, G. H. Seo, B. J. Choi, S. Kim, Y. G. Kim, Y. H. Youn, and E. P. Dever, 2009: Connectivity among straits of the northwest Pacific marginal seas. *J. Geophys. Res. Oceans*, **114**, C06018, https://doi.org/10.1029/2008JC005218.

Cui, Y. L., and T. Senjyu, 2010: Interdecadal oscillations in the Japan Sea proper water related to the Arctic Oscillation. *J. Oceanogr.*, **66**, 337–348, https://doi.org/10.1007/s10872-010-0030-z.

Cunningham, S. A., and R. Marsh, 2010: Observing and modeling changes in the Atlantic MOC. *Wiley Interdiscip. Rev.: Climate Change*, **1**, 180–191, https://doi.org/10.1002/wcc.22.

Fukudome, K., J. H. Yoon, A. Ostrovskii, T. Takikawa, and I. S. Han, 2010: Seasonal volume transport variation in the Tsushima Warm Current through the Tsushima Straits from 10 years of ADCP observations. *J. Oceanogr.*, **66**, 539–551, https://doi.org/10.1007/s10872-010-0045-5.

Han, M., I. Kamenkovich, T. Radko, and W. E. Johns, 2013: Relationship between air–sea density flux and isopycnal meridional overturning circulation in a warming climate. *J. Climate*, **26**, 2683–2699, https://doi.org/10.1175/JCLI-D-11-00682.1.

Han, S., N. Hirose, N. Usui, and Y. Miyazawa, 2016: Multi-model ensemble estimation of volume transport through the straits of the East/Japan Sea. *Ocean Dyn.*, **66**, 59–76, https://doi.org/10.1007/s10236-015-0896-9.

Ichiye, T., 1984: Some problems of circulation and hydrography of the Japan Sea and the Tsushima current. *Ocean Hydrodynamics of the Japan and East China Seas*, Elsevier, 15–54.

Kamenkovich, I., and T. Radko, 2011: Role of the Southern Ocean in setting the Atlantic stratification and meridional overturning

circulation. *J. Mar. Res.*, **69**, 277–308, https://doi.org/10.1357/002224011798765286.

Kang, D.-J., S. Park, Y.-G. Kim, K. Kim, and K.-R. Kim, 2003: A Moving-Boundary Box Model (MBBM) for oceans in change: An application to the East/Japan Sea. *Geophys. Res. Lett.*, **30**, 1299, https://doi.org/10.1029/2002GL016486.

Kim, C.-H., and J.-H. Yoon, 1999: A numerical modeling of the upper and the intermediate layer circulation in the East Sea. *J. Oceanogr.*, **55**, 327–345, https://doi.org/10.1023/A:1007837212219.

Kim, K., and J. Chung, 1984: On the salinity-minimum and dissolved oxygen-maximum layer in the East Sea (Sea of Japan). *Elsevier Oceanogr. Ser.*, **39**, 55–65, https://doi.org/10.1016/S0422-9894(08)70290-3.

——, K. R. Kim, Y. G. Kim, Y. K. Cho, D. J. Kang, M. Takematsu, and Y. Volkov, 2004: Water masses and decadal variability in the East Sea (Sea of Japan). *Prog. Oceanogr.*, **61**, 157–174, https://doi.org/10.1016/j.pocean.2004.06.003.

——, K.-I. Chang, D.-J. Kang, Y. H. Kim, and J.-H. Lee, 2008: Review of recent findings on the water masses and circulation in the East Sea (Sea of Japan). *J. Oceanogr.*, **64**, 721–735, https://doi.org/10.1007/s10872-008-0061-x.

Kim, K. R., G. Kim, K. Kim, V. Lobanov, V. Ponomarev, and A. Salyuk, 2002: A sudden bottom-water formation during the severe winter 2000–2001: The case of the East/Japan Sea. *Geophys. Res. Lett.*, **29**, 1234, https://doi.org/10.1029/2001GL014498.

Kim, Y.-G., and K. Kim, 1999: Intermediate waters in the East/Japan Sea. *J. Oceanogr.*, **55**, 123–132, https://doi.org/10.1023/A:1007877610531.

Kim, Y. H., Y. B. Kim, K. Kim, K. I. Chang, S. J. Lyu, Y. K. Cho, and W. J. Teague, 2006: Seasonal variation of the Korea strait bottom cold water and its relation to the bottom current. *Geophys. Res. Lett.*, **33**, L24604, https://doi.org/10.1029/2006GL027625.

Min, H. S., and C.-H. Kim, 2006: Water mass formation variability in the intermediate layer of the East Sea. *Ocean Sci. J.*, **41**, 255–260, https://doi.org/10.1007/BF03020629.

Miyazaki, M., 1953: On the water masses of the Japan Sea. *Bull. Hokkaido Reg. Fish. Res. Lab.*, **7**, 1–65.

Moriyasu, S., 1972: The Tsushima Current. *Kuroshio: Its Physical Aspects*, H. Stommel and K. Yoshida, Eds., University of Tokyo Press, 353–369.

Nam, S., S. T. Yoon, J. H. Park, Y. H. Kim, and K. I. Chang, 2016: Distinct characteristics of the intermediate water observed off the east coast of Korea during two contrasting years. *J. Geophys. Res. Oceans*, **121**, 5050–5068, https://doi.org/10.1002/2015JC011593.

Noh, S., and S. Nam, 2018: EC1, mooring time-series since 1996. SEANOE, accessed 5 December 2018, https://doi.org/10.17882/58134.

Noh, Y., and C. Jang, 1999: Large eddy simulation of open ocean deep convection with application to the deep water formation in the East Sea (Japan Sea). *J. Oceanogr.*, **55**, 347–367, https://doi.org/10.1023/A:1007889229058.

Park, J., and B. Lim, 2017: A new perspective on origin of the East Sea Intermediate water: Observations of Argo floats. *Prog. Oceanogr.*, **160**, 213–224, https://doi.org/10.1016/J.POCEAN.2017.10.015.

——, and S. Nam, 2018: Interannual variability of winter precipitation linked to upper ocean heat content off the east coast of Korea. *Int. J. Climatol.*, **38**, e1266–e1273, https://doi.org/10.1002/joc.5354.

Park, Y.-G., K.-H. Oh, K.-I. Chang, and M.-S. Suk, 2004: Intermediate level circulation of the southwestern part of the East/Japan Sea estimated from autonomous isobaric profiling floats. *Geophys. Res. Lett.*, **31**, L13213, https://doi.org/10.1029/2004GL020424.

Park, Y. G., A. Choi, Y. H. Kim, H. S. Min, J. H. Hwang, and S. H. Choi, 2010: Direct flows from the Ulleung Basin into the Yamato Basin in the East/Japan Sea. *Deep-Sea Res. I*, **57**, 731–738, https://doi.org/10.1016/j.dsr.2010.03.006.

——, J. H. Park, H. J. Lee, H. S. Min, and S. D. Kim, 2013: The effects of geothermal heating on the East/Japan Sea circulation. *J. Geophys. Res. Oceans*, **118**, 1893–1905, https://doi.org/10.1002/jgrc.20161.

Senjyu, T., H.-R. Shin, J.-H. Yoon, Z. Nagano, H.-S. An, S.-K. Byun, and C.-K. Lee, 2005: Deep flow field in the Japan/East Sea as deduced from direct current measurements. *Deep-Sea Res. II*, **52**, 1726–1741, https://doi.org/10.1016/J.DSR2.2003.10.013.

Seung, Y. H., 2005: Abyssal currents driven by a local wind forcing through deep mixed layer: Implication to the East Sea. *Ocean Sci. J.*, **40**, 101–107, https://doi.org/10.1007/BF03028590.

Seung, Y.-H., and J.-H. Yoon, 1995: Some features of winter convection in the Japan Sea. *J. Oceanogr.*, **51**, 61–73, https://doi.org/10.1007/BF02235936.

Speer, K., and E. Tziperman, 1992: Rates of water mass formation in the North Atlantic Ocean. *J. Phys. Oceanogr.*, **22**, 93–104, https://doi.org/10.1175/1520-0485(1992)022<0093:ROWMFI>2.0.CO;2.

Stouffer, R. J., and Coauthors, 2006: Investigating the causes of the response of the thermohaline circulation to past and future climate changes. *J. Climate*, **19**, 1365–1387, https://doi.org/10.1175/JCLI3689.1.

Takematsu, M., Z. Nagano, A. G. Ostrovski, K. Kim, and Y. Volkov, 1999: Direct measurements of deep currents in the northern Japan Sea. *J. Oceanogr.*, **55**, 207–216, https://doi.org/10.1023/A:1007842013257.

Takikawa, T., J. H. Yoon, and K. D. Cho, 2005: The Tsushima warm current through Tsushima Straits estimated from ferryboat ADCP data. *J. Phys. Oceanogr.*, **35**, 1154–1168, https://doi.org/10.1175/JPO2742.1.

Talley, L., and Coauthors, 2006: Japan/East Sea water masses and their relation to the sea's circulation. *Oceanography*, **19**, 32–49, https://doi.org/10.5670/oceanog.2006.42.

Talley, L. D., V. Lobanov, V. Ponomarev, A. Salyuk, P. Tishchenko, I. Zhabin, and S. Riser, 2003: Deep convection and brine rejection in the Japan Sea. *Geophys. Res. Lett.*, **30**, 1159, https://doi.org/10.1029/2002GL016451.

Tanaka, K., 2014: Formation of bottom water and its variability in the northwestern part of the Sea of Japan. *J. Geophys. Res. Oceans*, **119**, 2081–2094, https://doi.org/10.1002/2013JC009456.

Teague, W., and Coauthors, 2005: Observed deep circulation in the Ulleung Basin. *Deep-Sea Res. II*, **52**, 1802–1826, https://doi.org/10.1016/J.DSR2.2003.10.014.

Wunsch, C., 2002: What is the thermohaline circulation? *Science*, **298**, 1179–1181, https://doi.org/10.1126/science.1079329.

Yoon, J.-H., K. Abe, T. Ogata, and Y. Wakamatsu, 2005: The effects of wind-stress curl on the Japan/East Sea circulation. *Deep-Sea Res. II*, **52**, 1827–1844, https://doi.org/10.1016/J.DSR2.2004.03.004.

Yoon, S. T., and Coauthors, 2018: Re-initiation of bottom water formation in the East Sea (Japan Sea) in a warming world. *Sci. Rep.*, **8**, 1576, https://doi.org/10.1038/s41598-018-19952-4.

Yoshikawa, Y., T. Awaji, and K. Akitomo, 1999: Formation and circulation processes of intermediate water in the Japan Sea. *J. Phys. Oceanogr.*, **29**, 1701–1722, https://doi.org/10.1175/1520-0485(1999)029<1701:FACPOI>2.0.CO;2.

Yun, J. Y., L. Magaard, K. Kim, C. W. Shin, C. Kim, and S. K. Byun, 2004: Spatial and temporal variability of the North Korean Cold Water leading to the near-bottom cold water intrusion in Korea Strait. *Prog. Oceanogr.*, **60**, 99–131, https://doi.org/10.1016/j.pocean.2003.11.004.